Geophysical Research Letters

RESEARCH LETTER
10.1029/2018GL078103

Time-Dependent Compaction as a Mechanism for Regular Stick-Slips

M. P. A. van den Ende[1] and A. R. Niemeijer[1]

[1] High Pressure and Temperature Laboratory, Department of Earth Sciences, Utrecht University, Utrecht, Netherlands

Key Points:
- For the first time, regular stick-slips are produced in discrete element method simulations
- The interplay between time-dependent compaction and granular flow is a key mechanism for generating frictional instabilities
- A new interpretation of stick-slips facilitates extrapolation of laboratory results to natural in situ conditions

Supporting Information:
- Supporting Information S1

Correspondence to:
M. P. A. van den Ende,
m.p.a.vandenende@uu.nl

Citation:
van den Ende, M. P. A., & Niemeijer, A. R. (2018). Time-dependent compaction as a mechanism for regular stick-slips. *Geophysical Research Letters*, *45*, 5959–5967. https://doi.org/10.1029/2018GL078103

Received 28 MAR 2018
Accepted 31 MAY 2018
Accepted article online 11 JUN 2018
Published online 22 JUN 2018

Abstract Owing to their destructive potential, earthquakes receive considerable attention from laboratory studies. In friction experiments, stick-slips are studied as the laboratory equivalent of natural earthquakes, and numerous attempts have been made to simulate stick-slips numerically using the discrete element method (DEM). However, while laboratory stick-slips commonly exhibit regular stress drops and recurrence times, stick-slips generated in DEM simulations are highly irregular. This discrepancy highlights a gap in our understanding of stick-slip mechanics, which propagates into our understanding of earthquakes. In this work, we show that regular stick-slips emerge in DEM when time-dependent compaction by pressure solution is considered. We further show that the stress drop and recurrence time of stick-slips are directly controlled by the kinetics of pressure solution. Since compaction is known to operate in faults, this mechanism for frictional instabilities directly relates to natural seismicity.

Plain Language Summary Earthquakes have a big impact on the society and are therefore intensively studied in laboratory settings. The study of laboratory-scale earthquakes, the so-called stick-slips, generates new insights into the origin and behavior of earthquakes in nature. At present, computer simulations of stick-slips have not been able to reproduce prominent laboratory observations, which shows that the origin of stick-slips, and of natural earthquakes, is not yet fully understood. In this work, we present computer simulations that succeed to reproduce the laboratory observations, thereby revealing that time-dependent compaction is of great importance to stick-slips and natural earthquakes. These results help to further understand the complex behavior of earthquakes in nature.

1. Introduction

The risk to society posed by earthquakes worldwide calls for a thorough understanding of the mechanisms driving earthquake nucleation and rupture propagation. Stick-slips have long been recognized as being the laboratory analog for natural earthquakes (Brace & Byerlee, 1966) and are therefore intensively studied to uncover the processes involved in unstable frictional sliding of rock interfaces and of fault gouges, the granular product of rock wear due to fault motion (Anthony & Marone, 2005; Leeman et al., 2016; Scuderi et al., 2014). The frictional strength and stability of gouges is often interpreted in a framework of granular flow and force transmission within the aggregate. Most notably, models describing the stability of the so-called force chains (discrete groups of grains that support the majority of the imposed load; Cates et al., 1998; Farr et al., 1997) have received much attention (e.g., Rechenmacher et al., 2010; Tordesillas et al., 2011). During the "stick"-phase, when the sample is locked and accumulates elastic strain, the force chains support the external load and sliding of grains is prohibited. When the yield strength of the aggregate is reached, force chains start to collapse or buckle, and a cascade of these events results in macroscopic sample failure, followed by accelerated (unstable) slip. This cycle of formation and destruction of force chains is thought to explain the existence of frictional instabilities (Daniels & Hayman, 2008; Tordesillas et al., 2009).

The presence of force chains within dry granular aggregates has been demonstrated both experimentally (Daniels & Hayman, 2008; Hayman et al., 2011) and numerically (Aharonov & Sparks, 2002, 2004; Mair & Hazzard, 2007), and force chain collapse has been positively correlated with the onset of frictional instabilities (Daniels & Hayman, 2008). Many numerical studies employ the discrete element method (DEM) for this particular problem (e.g., Ferdowsi et al., 2013; Morgan, 2004; Tordesillas et al., 2011), a numerical technique that is ideally suited to investigate the behavior of aggregates with a large number of degrees of freedom. By implementing the appropriate physical interactions between particles, DEM can be employed to simulate

and generalize the complex behavior observed in the laboratory, and test hypotheses regarding the mechanisms of stick-slips. Since the conceptual model of force chain collapse described above is entirely seated on elastic-frictional interactions between discrete particles, standard DEM formulations incorporating these interactions ought to be capable of reproducing the stick-slip behavior as observed in the laboratory. However, many DEM studies report only irregular stick-slip behavior, that is, stress drops of highly variable magnitude and recurrence time (Aharonov & Sparks, 2004; Dorostkar et al., 2017; Ferdowsi et al., 2013; Morgan, 2004), while most laboratory studies report regular stick-slips (Anthony & Marone, 2005; Leeman et al., 2016; Mair et al., 2002; Scuderi et al., 2016; Tinti et al., 2016). This discrepancy reveals a gap in our understanding of stick-slip and earthquake mechanics and calls for a reappraisal of the force chain conceptual model.

In this study, we show that regular stick-slips with near-constant recurrence time and stress drop can be reproduced in DEM when fluid-rock interactions are incorporated. Following Niemeijer and Spiers (2007) and Chen and Spiers (2016), we consider the interplay between dilatant granular flow and compaction by intergranular pressure solution, which has been proposed by these authors as a mechanism for velocity-weakening behavior, a requirement for stick-slip behavior (Gu et al., 1984; Ruina, 1983). By employing the implementation of pressure solution in DEM by Van den Ende, Marketos, et al. (2018), we simulate unstable frictional sliding of fault gouges while systematically varying the kinetics of pressure solution, and we investigate the effect of these fluid-rock interactions on the frictional behavior of the gouge. Simulations with appreciable pressure solution kinetics display stick-slips with regular recurrence time and stress drop, demonstrating that the interplay between dilatant granular flow and time-dependent compaction leads to periodic unstable sliding. We subsequently relate the frictional properties of the aggregate to the internal distribution of force and stress and show that compaction by pressure solution leads to a more diffuse transmission of stress, so that the stability of individual force chains no longer controls the overall sliding stability of the aggregate. Instead, the stress drop and recurrence time of stick-slips (and earthquakes by analogy) are directly controlled by compaction induced by pressure solution. These results imply that the analysis of force chains may not provide the necessary insights relevant for understanding the frictional behavior of natural faults that undergo fluid-rock interactions.

2. Numerical Methods

To investigate the effect of pressure solution creep on stick-slip behavior, we simulate laboratory biaxial shear tests numerically using the DEM (Cundall & Strack, 1979). We employ the open-source 3-D DEM software package granular LAMMPS (Landry et al., 2003; Plimpton, 1995), which was modified by Marketos (2013) and by Van den Ende, Marketos, et al. (2018). The DEM approach is summarized in supporting information S1 (Guo & Morgan, 2006; Hanley et al., 2015; Jiang et al., 2010; Mair & Abe, 2008; Scholtès & Donzé, 2012). For a detailed description of the numerical method and the implementation of intergranular pressure solution in DEM, the reader is referred to Van den Ende, Marketos, et al. (2018). All simulation parameters reported below and in Table S2 are presented in their physical dimensions for easy comparison with laboratory values (see Van den Ende, Marketos, et al., 2018, for details of the adopted scaling procedure).

2.1. Basic Model Approach

During each time step of a DEM simulation, the forces of interaction between particles in contact are calculated for each particle in the virtual aggregate, and their positions are updated through integration of Newton's laws of motion. In addition to commonly adopted elastic and frictional interactions between particles, dissolution of stressed particle contacts by pressure solution is simulated by altering the contact model for the normal force F_n as follows:

$$F_n = k_n \left(\Delta x_t - \delta \right) \tag{1}$$

where k_n is the contact normal stiffness and Δx_t is the total overlap between two particles in contact, computed as the distance between their centroids minus the sum of their radii. Over time, the dissolved overlap δ increases as material dissolves from the stressed interface, causing convergence of the particle centroids at a rate $2V_{ps}$, where V_{ps} is given by the following:

$$V_{ps} = Z_{ps} \frac{\pi F_n}{A_c^2} \tag{2}$$

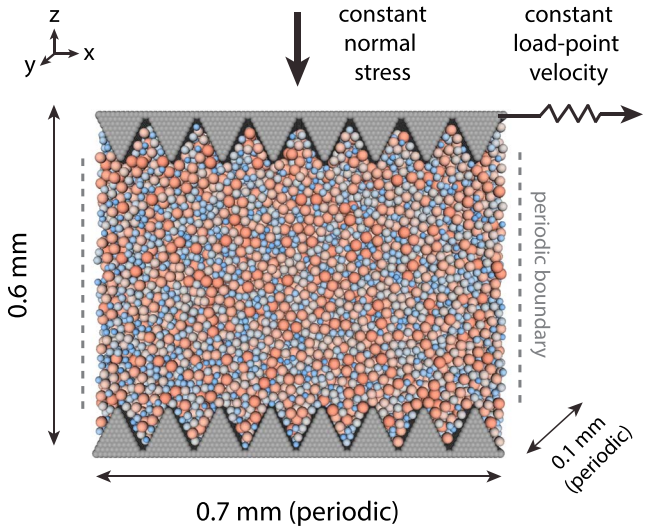

Figure 1. Visualization of the discrete element method sample prior to the steady-state sliding phase. To visually distinguish the particles in the gouge, the particles are color coded according to their diameter (in the range of 10 to 20 μm), with warmer colors corresponding to larger sizes.

Here Z_{ps} is a kinetic constant and A_c is the circular area of intersection of the two spheres in contact. For a given F_n, Δx_t will increase over time to compensate for the increase in δ, hence resulting in particle convergence and overall densification of the system.

By adopting equation (2), it is assumed that the system is closed with respect to the solid mass (i.e., no long-range mass transport is permitted) and that the solute concentration remains constant. The precipitation of material on the unstressed pore walls is not modelled explicitly, thereby neglecting a small contribution of precipitation to growth of the particle contacts.

2.2. Model Setup

First, a sample is generated consisting of 10,000 particles, sampled from a uniform size distribution in the range of 10 to 20 μm , enclosed in the vertical direction by two rigid toothed pistons (see Figure 1). In the horizontal directions, periodic boundaries are employed. During the simulations, a constant, servo-controlled normal stress of $\sigma_n = 5$MPa is imposed onto the gouge by the top piston. After application of the normal load, the top piston is pulled by a virtual spring in the x-direction at a rate of 10 μm/s to simulate gouge deformation in a biaxial shear configuration. The shear force exerted by the aggregate on the top piston is calculated each time step, from which the shear stress τ is obtained as the shear force divided by the nominal top surface area of the piston.

Each simulation consists of two phases: In the steady-state sliding phase, the sample is deformed for 100 s with a high stiffness of the virtual spring, so that sliding is stable and a steady-state shear stress is achieved. Then the stiffness of the spring is instantaneously lowered to a value that permits unstable sliding (see Gu et al., 1984; Ruina, 1983), and deformation is continued for another 1,000 s, during which stick-slips are generated. This procedure is repeated for different values of the pressure solution kinetic constant Z_{ps} of 0, 1.05×10^{-28}, 1.05×10^{-27}, and 5.25×10^{-28} $m^3 \cdot Pa^{-1} \cdot s^{-1}$. A value of $Z_{ps} = 0$ indicates that pressure solution is inactive and corresponds to previous DEM studies where only elastic-frictional interactions have been considered. Higher values of $Z_{ps} > 0$ indicate faster rates of pressure solution creep, with the maximum value of 5.25×10^{-28} $m^3 \cdot Pa^{-1} \cdot s^{-1}$ corresponding to the kinetics of halite (NaCl) at room temperature (Spiers et al., 1990). A summary of the DEM parameter values is given in Table S2.

During each simulation, the volumetric sample response is continuously monitored. This is done by calculating the bulk sample porosity ϕ from the total mass of the particles present in the system, and the total volume occupied by the sample enclosed by the simulation domain boundaries. The total sample volume is corrected for the volume occupied by the pistons, so that estimates of porosity represent the porosity of the gouge layer itself.

2.3. Contact Stress Distributions

To better apprehend the effect of nonzero Z_{ps} on the state of the aggregate, it is useful to consider the local distribution of particle contact stresses. To this end, we calculate for each particle contact the maximum compressive force in the direction of shear as $f_c = \sqrt{f_x^2 + f_z^2}$, where f_i is the component of force along the i-coordinate, with $i = x$ being the direction of shear, and $i = z$ being the vertical (shear plane normal) direction. The contact stress is accordingly calculated as $\sigma = f_c / A_c$, with A_c being the area of the circular intersection between two overlapping spheres. We compute probability density functions of σ and f_c using the Python NumPy package (Oliphant, 2006).

3. Results

3.1. Steady-State Deformation

During the steady-state sliding stage (at high spring stiffness), it is observed that the steady-state macroscopic coefficient of friction ($\mu = \tau / \sigma_n$) increases with increasing pressure solution kinetics (Z_{ps}), concurrent with a decreasing overall porosity (see Figure 2). Furthermore, simulations with higher values of Z_{ps} display smoother friction curves, with fewer and smaller load drops during sliding. For all simulations

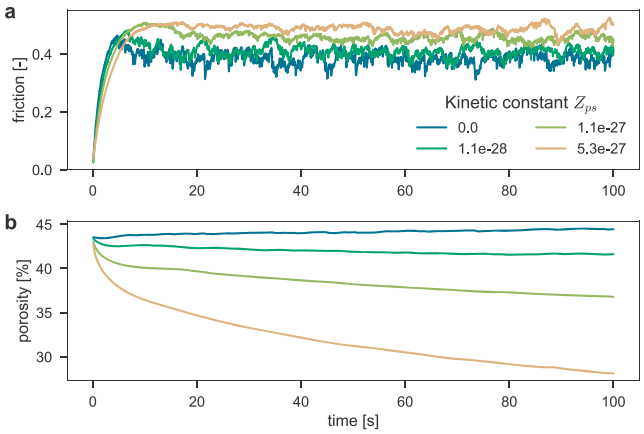

Figure 2. Time series of the steady-state sliding phase, for different values of the pressure solution kinetic constant Z_{ps}. (a) Apparent coefficient of friction ($\mu = \tau/\sigma_n$); (b) the volumetric response of each sample, represented by the bulk-averaged porosity.

with $Z_{ps} > 0$, the net volumetric behavior is compactive, with only the simulation with $Z_{ps} = 0$ being dilatant. It should be taken into account, however, that these simulations experience localization of shear strain. In the simulation with $Z_{ps} = 0$, the passive region of the sample is stationary, so that the observed dilatancy is fully attributable to granular flow in the active region. In the simulations with $Z_{ps} > 0$, the passive region continues to compact by pressure solution in the absence of dilatant granular flow, so that the volumetric signal of the active region is obscured by the compaction of the bulk sample.

3.2. Unstable Sliding Behavior

When the loading spring stiffness is instantaneously lowered, all samples begin to undergo stick-slip cycles (Figure 3). The stick-slip behavior of the simulation with $Z_{ps} = 0$ is exemplary to stick-slips commonly observed in DEM, exhibiting stress drops of highly variable recurrence time and magnitude. This is similarly reflected by the volumetric response of the sample, showing irregular and nonsystematic timing of compaction and dilatation at porosities near 45%. There is no indication that the stick-slip behavior of the simulation with $Z_{ps} = 0$ will eventually evolve towards a more regular, repeating stick-slip sequence.

By contrast, all simulations with $Z_{ps} > 0$ show a pattern of periodically repeating stick-slips, all exhibiting a near-constant stress drop after a brief run-in of a few cycles. Simulations with higher values of Z_{ps} show longer recurrence times and correspondingly larger stress drops. The sample volumetric behavior mirrors that of the friction coefficient, showing compaction during the stick-phase, and rapid dilatation during the slip-phase. Due to localization, the behavior is net compactive, but the repetitive succession of compaction during the stick and dilatation during slip is persistent. As compaction of the bulk gouge decelerates with

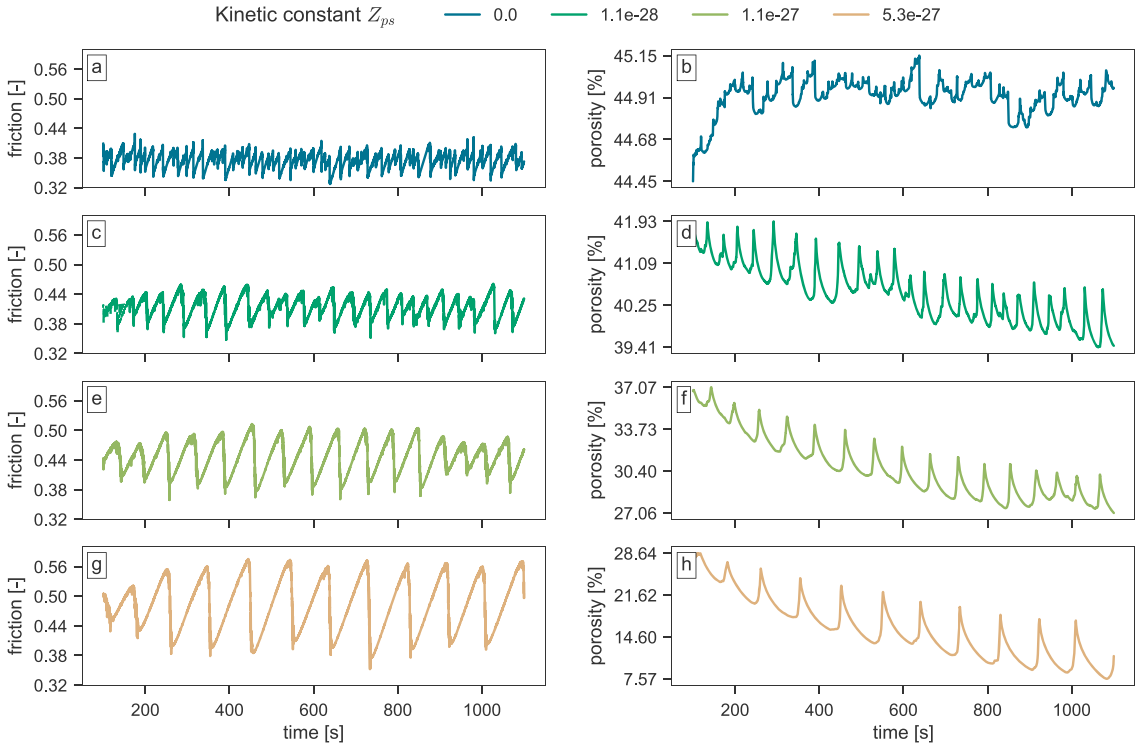

Figure 3. Time series of stick-slip behavior for all simulations. Left panels: coefficient of friction (τ/σ_n); right panels: sample porosity. The values of the pressure solution kinetic constant Z_{ps} are as indicated in the figure legend. Note that the porosity data is plotted on different vertical scales.

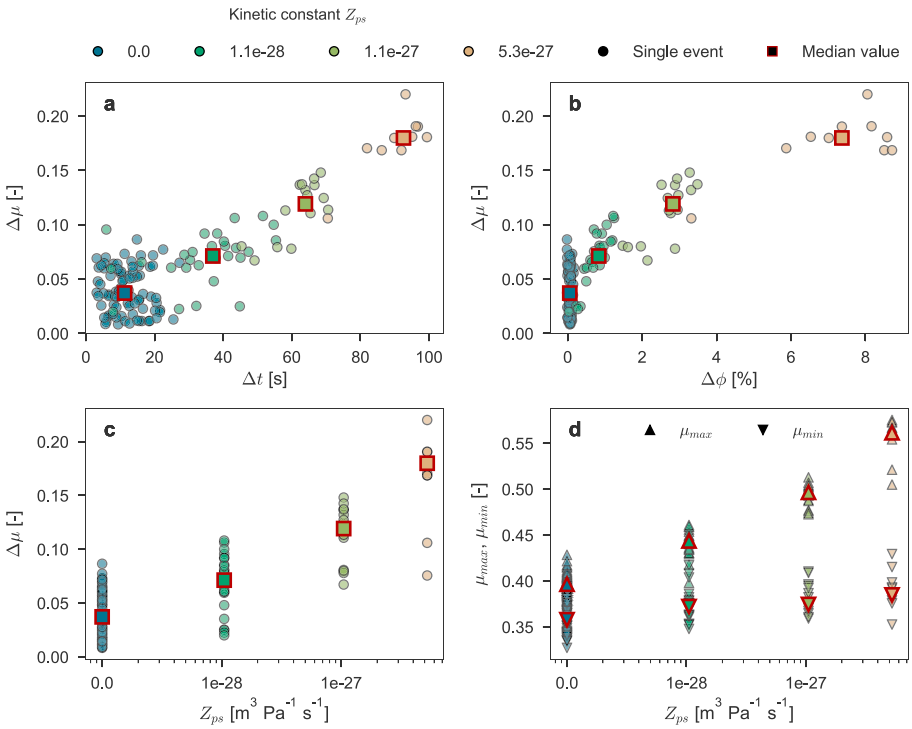

Figure 4. Overview of stick-slip characteristics. (a) Friction drop $\Delta\mu$ as a function of preceding stick duration Δt; (b) friction drop $\Delta\mu$ as a function of the maximum dilatancy $\Delta\phi$ during slip; (c) friction drop $\Delta\mu$ as a function of the pressure solution kinetic constant Z_{ps}; (d) peak and residual friction for each slip event as a function of Z_{ps}. Note that the data for $Z_{ps} = 0$ are plotted at an arbitrary position on the logarithmic x-axis in panels (c) and (d).

decreasing porosity, volumetric response of the active zone becomes more prominent in the porosity evolution (Figure 3h). Overall, the volumetric behavior of the passive zone does not influence the stick-slip cycle behavior.

The sample stick-slip behavior can be characterized by considering the friction drop $\Delta\mu$, the preceding stick duration Δt, and the maximum dilatancy $\Delta\phi$ associated with each slip event (Figure 4). Particularly for the two simulations with the lowest values of Z_{ps}, there is substantial scatter present in the data set, but the median values of each data set consistently show positive relations between each of the aforementioned quantities. What is also clearly noticeable in Figures 4a and 4b is that there is no clear relationship between stress drop and recurrence time on the one hand, and dilatation on the other for the simulation with $Z_{ps} = 0$, as noted earlier (see Figures 3a and 3b). With increasing value of $Z_{ps} > 0$, the amount of compaction (and accordingly the amount of dilatation) increases, leading to a larger friction drop and recurrence time.

4. Discussion

4.1. Comparison With Previous Work

Most commonly, 3-D DEM studies of biaxial shear deformation of dry aggregates observe a macroscopic friction coefficient in the range of 0.2–0.5 (e.g., Dorostkar et al., 2017; Guo & Morgan, 2004; Mair & Hazzard, 2007). This value has been found to be controlled by geometric quantities such as particle dimensionality (Frye & Marone, 2002) and particle shape (Guo & Morgan, 2004). Our values of friction fall within this range, though our results also show that higher values of Z_{ps} systematically produce higher friction values. Likewise, the volumetric sample response for the simulation with $Z_{ps} = 0$ is broadly similar to previous DEM studies, exhibiting irregular excursions in sample porosity around a given mean value during stick-slip (e.g., Dorostkar et al., 2017; Morgan, 2004). By contrast, the simulations with $Z_{ps} > 0$ show a much clearer relation between stress and porosity during each stick-slip cycle, in a way that has not been previously reported.

4.2. Contact Stress Distribution

To characterize the distribution of stresses and forces within the aggregate for the different values of Z_{ps}, we compute probability density functions of the maximum compressive contact force (f_c) and stress

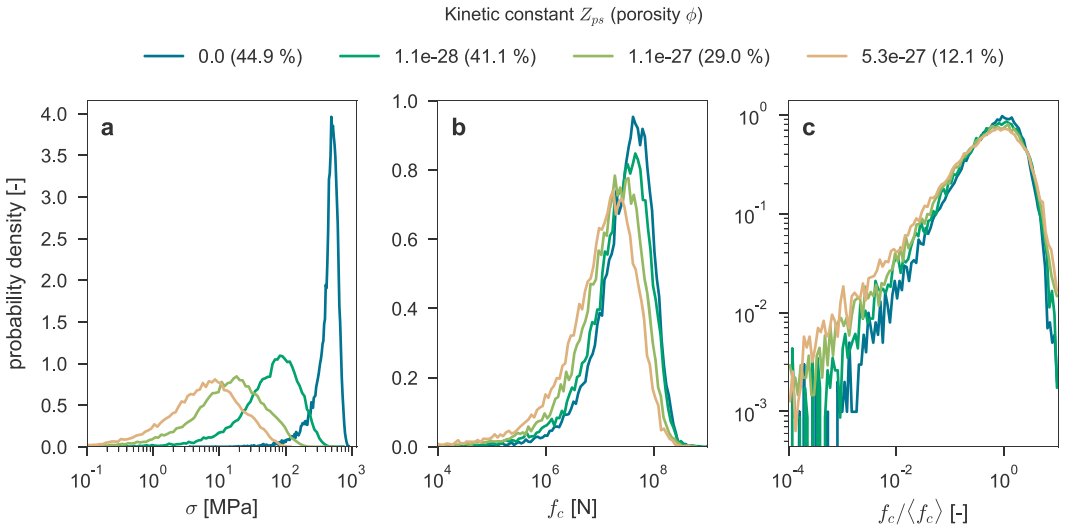

Figure 5. Contact stress and force distributions. (a) Maximum compressive contact stress $\sigma = f_c/A_c$; (b) maximum compressive contact force f_c; (c) contact force f_c normalized by the bulk mean value $\langle f_c \rangle$. The value of the kinetic constant Z_{ps} and porosity ϕ are as indicated in the legend.

($\sigma = f_c/A_c$)–see Figure 5. As opposed to absolute probability, the probability density may exceed a value of 1, with higher values indicating a larger proportion of particle contacts exhibiting a particular value of force or stress. For a unimodal probability density function, lower peak values imply a wider distribution.

When compaction by pressure solution is absent ($Z_{ps} = 0$), the contact stresses cluster narrowly around the mean value (Figure 5a). The contact stress distributions as seen in simulations with $Z_{ps} > 0$ are markedly different from that seen in the simulation with $Z_{ps} = 0$. Instead of exhibiting a narrow peak near the mean value, the contact stress distribution becomes wider with increasing Z_{ps} and shifts towards lower values. This can also be observed (although to a lesser extent) when considering the contact forces (Figure 5b). The widening of the distributions with increasing Z_{ps} implies that the stress becomes more diffusely distributed throughout the aggregate, which has been argued to stabilize force chains present in the system and to inhibit unstable sliding (Mair et al., 2002). Lastly, the distribution of contact forces (Figure 5c), normalized by the bulk mean value $\langle f_c \rangle$ of each sample, is broadly similar to what has been reported by previous particle-based studies (e.g., Aharonov & Sparks, 2004; Radjai et al., 1996, their Figure 3).

The distribution of contact stresses when pressure solution is active can be explained by considering the negative feedback loop induced by pressure solution creep: When the stress on the contact is locally high, the rate of pressure solution is fast and so the contact area grows rapidly due to particle convergence. As a result, local concentrations of contact stress diminish and cease to exist. This has been demonstrated quantitatively by Van den Ende, Marketos, et al. (2018) for uniaxially compacting aggregates. Overall, pressure solution negatively impacts the formation of isolated force chains, so that force chain collapse is unlikely to constitute the observed stick-slip behavior.

4.3. The Origin of Regular Stick-Slips

Classically, conceptual models for the occurrence of (repeating) earthquakes revolve around the notion that faults strengthen during interseismic times and that the instability (the earthquake) occurs when the tectonic stress exceeds the shear strength of the fault. If laboratory stick-slips are truly analogous to natural earthquakes, then the same mechanism is expected to apply for stick-slips. However, at the scale of a laboratory aggregate, the force chain collapse model is generally preferred, which does not involve time-dependent strengthening as envisioned for natural seismic cycles.

In our DEM simulations, we observe prominent compaction during the stick-phase and dilatation during the slip-phase. As has been demonstrated by laboratory friction tests (Karner & Marone, 2001; Richardson & Marone, 1999) and by analytical models (Chen & Spiers, 2016), densification is positively correlated with aggregate strength, and so the observed compaction translates into a time-dependent increase in shear strength. Due to continuous loading at the load point, the stress exerted on the aggregate increases during

the stick-phase. When the shear stress acting on the gouge exceeds the aggregate strength, an instability is triggered and the sample slips. During accelerated slip, granular flow induces dilatation and weakening in the sample, and the cycle repeats. This conceptual model of a stick-slip cycle is generally compatible with present models for the natural seismic cycle (Sleep & Blanpied, 1992; Van den Ende, Chen, et al., 2018) and is an outcome of the microphysical models proposed by Niemeijer and Spiers (2007) and Chen and Spiers (2016), which are seated on the same physical principles (pressure solution and granular flow) as the DEM simulations presented here. One key aspect in this conceptual model is the process of gouge compaction during the stick-phase.

When pressure solution is operative, time-dependent strengthening of the aggregate by compaction is expected to dominate over local variations in packing density and stress distribution, so that the overall stress drop and recurrence time are one-sidedly controlled by the volumetric evolution of the aggregate (i.e., compaction during the stick-phase, and dilatation during the slip-phase). As a result, the stress drop and recurrence time are regular in magnitude. Conversely, in the absence of compaction by pressure solution, local variations in packing density and contact stress (and correspondingly the presence of isolated force chains) are expected to determine the irregular stick-slip behavior as seen when $Z_{ps} = 0$, as there exists no mechanism to counteract or dominate over the local random fluctuations.

The results presented here indicate that a time-dependent strengthening mechanism is required to explain the stick-slip behavior observed in laboratory experiments. In our DEM simulations, this strengthening mechanism is provided by time-dependent compaction by pressure solution, but alternative processes, such as microcracking (Atkinson, 1984; Brantut et al., 2013) or plastic creep (Dieterich & Kilgore, 1994; Scuderi et al., 2014), could be considered depending on the test material and conditions. In addition to an increase in the coefficient of friction, cohesion (possibly facilitated by pressure solution; Angevine et al., 1982) could contribute to the time-dependent strengthening of fault rocks, as has been experimentally demonstrated by, for example, Tenthorey and Cox (2006). Our results imply that such time-dependent strengthening mechanisms likely play a major role in controlling the frictional behavior of natural faults.

5. Implications and Concluding Remarks

Numerous field geological studies have convincingly demonstrated that pressure solution creep and granular flow are dominant deformation mechanisms within faults at seismogenic depths (Chester et al., 1993; Holdsworth et al., 2011; Smeraglia et al., 2017) — see also Gratier and Gueydan (2007) and references therein. These deformation mechanisms have similarly been identified in laboratory friction experiments performed under (seismogenic) conditions that favor pressure solution creep (Bos et al., 2000; Chen et al., 2015; Niemeijer & Spiers, 2006) and have been argued to govern velocity-weakening behavior and stick-slip instability nucleation (Chen & Spiers, 2016; Niemeijer & Spiers, 2007). Our simulations show that the interplay between dilatant granular flow and nondilatant pressure solution indeed generates stick-slips as reported by laboratory studies, as envisioned in microphysical models, and as supported by field observations.

Encouraged by the above, we will now broaden our interpretation of the mechanics of stick-slip to discuss the implications for natural seismicity. In our simulations with constant displacement rate, the kinetics of pressure solution control the recurrence time and stress drop of the unstable slip events through the amount of compaction achieved during the interseismic period and correspondingly the amount of dilatation during accelerated slip. This offers important constraints on the stress drop in the absence of dynamic weakening (see Tullis, 2007), which is highly relevant for slow slip events (Gomberg, 2010; Rogers & Dragert, 2003) and (induced) microseismicity. Furthermore, if the kinetics of pressure solution control the recurrence interval of natural earthquakes, spatial variations in pressure solution rates due to variable temperature, mineralogy, and pore fluid chemistry will produce spatially heterogeneous seismicity distributions. Therefore, laboratory experiments designed to quantifying the rate of gouge compaction (such as uniaxial compaction tests, e.g., Pluymakers & Spiers, 2014) will provide constraints on the amount of compaction expected during interseismic times under in situ fault conditions, which in turn may grant important insights into spatial and/or temporal variability of natural earthquakes. Laboratory estimates of the kinetics of pressure solution (i.e., Z_{ps}) can be used as direct input for numerical models.

Lastly, the capability of DEM to capture the mechanics of earthquake nucleation strongly solicits for a detailed investigation of the nucleation process using this numerical method. Among others, two potential avenues

of investigation are the study of precursory phenomena (e.g., Ferdowsi et al., 2013), and the mechanical effects of an (undrained) fluid phase (e.g., Catalano et al., 2014; Dorostkar et al., 2017). Both of these subjects are challenging to address in laboratory experiments, as details of the local microstructure, state of stress, and fluid pressure are generally not available. In this way, the DEM approach presented in this work offers means to complement previous field, laboratory, and model studies concerning earthquake nucleation.

Acknowledgments
The authors thank Å. Fagereng, D. Elsworth, and E. Aharonov for their constructive comments. This project is supported by the European Research Council (ERC), grant 335915, and by the NWO Vidi grant 854.12.001 awarded to A. R. Niemeijer. Model data and Python scripts used to generate the data figures are available as Van den Ende (2018): Discrete Element Method model data of biaxial shear deformation. GFZ Data Services. http://doi.org/10.5880/fidgeo.2018.008.

References

Aharonov, E., & Sparks, D. (2002). Shear profiles and localization in simulations of granular materials. *Physical Review E*, *65*, 1–12. https://doi.org/10.1103/PhysRevE.65.051302

Aharonov, E., & Sparks, D. (2004). Stick-slip motion in simulated granular layers. *Journal of Geophysical Research*, *109*, B09306. https://doi.org/10.1029/2003JB002597

Angevine, C. L., Turcotte, D. L., & Furnish, M. D. (1982). Pressure solution lithification as a mechanism for the stick-slip behavior of faults. *Tectonics*, *1*(2), 151–160. https://doi.org/10.1029/TC001i002p00151

Anthony, J. L., & Marone, C. (2005). Influence of particle characteristics on granular friction. *Journal of Geophysical Research: Solid Earth*, *110*, B08409. https://doi.org/10.1029/2004JB003399

Atkinson, B. K. (1984). Subcritical crack growth in geological materials. *Journal of Geophysical Research*, *89*(B6), 4077–4114. https://doi.org/10.1029/JB089iB06p04077

Bos, B., Peach, C. J., & Spiers, C. J. (2000). Frictional-viscous flow of simulated fault gouge caused by the combined effects of phyllosilicates and pressure solution. *Tectonophysics*, *327*, 173–194.

Brace, W. F., & Byerlee, J. D. (1966). Stick-slip as a mechanism for earthquakes. *Science*, *153*(3739), 990–992. https://doi.org/10.1126/science.153.3739.990

Brantut, N., Heap, M. J., Meredith, P. G., & Baud, P. (2013). Time-dependent cracking and brittle creep in crustal rocks: A review. *Journal of Structural Geology*, *52*, 17–43. https://doi.org/10.1016/j.jsg.2013.03.007

Catalano, E., Chareyre, B., & Barthélémy, E. (2014). Pore-scale modeling of fluid-particles interaction and emerging poromechanical effects. *International Journal for Numerical and Analytical Methods in Geomechanics*, *38*(1), 51–71. https://doi.org/10.1002/nag.2198

Cates, M. E., Wittmer, J. P., Bouchaud, J.-P., & Claudin, P. (1998). Jamming, force chains, and fragile matter. *Physical Review Letters*, *81*(9), 1841–1844. https://doi.org/10.1103/PhysRevLett.81.1841

Chen, J., & Spiers, C. J. (2016). Rate and state frictional and healing behavior of carbonate fault gouge explained using microphysical model. *Journal of Geophysical Research: Solid Earth*, *121*, 8642–8665. https://doi.org/10.1002/2016JB013470

Chen, J., Verberne, B. A., & Spiers, C. J. (2015). Interseismic re-strengthening and stabilization of carbonate faults by "non-Dieterich" healing under hydrothermal conditions. *Earth and Planetary Science Letters*, *423*, 1–12. https://doi.org/10.1016/j.epsl.2015.03.044

Chester, F. M., Evans, J. P., & Biegel, R. L. (1993). Internal structure and weakening mechanisms of the San Andreas Fault. *Journal of Geophysical Research*, *98*(B1), 771–786. https://doi.org/10.1029/92JB01866

Cundall, P. A., & Strack, O. D. L. (1979). A discrete numerical model for granular assemblies. *Géotechnique*, *29*(1), 47–65. https://doi.org/10.1680/geot.1979.29.1.47

Daniels, K. E., & Hayman, N. W. (2008). Force chains in seismogenic faults visualized with photoelastic granular shear experiments. *Journal of Geophysical Research*, *113*, B11411. https://doi.org/10.1029/2008JB005781

Dieterich, J. H., & Kilgore, B. D. (1994). Direct observation of frictional contacts: New insights for state-dependent properties. *Pure and Applied Geophysics PAGEOPH*, *143*(1-3), 283–302. https://doi.org/10.1007/BF00874332

Dorostkar, O., Guyer, R. A., Johnson, P. A., Marone, C., & Carmeliet, J. (2017). On the role of fluids in stick-slip dynamics of saturated granular fault gouge using a coupled computational fluid dynamics-discrete element approach. *Journal of Geophysical Research: Solid Earth*, *122*, 3689–3700. https://doi.org/10.1002/2017JB014099

Farr, R. S., Melrose, J. R., & Ball, R. C. (1997). Kinetic theory of jamming in hard-sphere startup flows. *Physical Review E*, *55*(6), 7203–7211. https://doi.org/10.1103/PhysRevE.55.7203

Ferdowsi, B., Griffa, M., Guyer, R. A., Johnson, P. A., Marone, C., & Carmeliet, J. (2013). Microslips as precursors of large slip events in the stick-slip dynamics of sheared granular layers: A discrete element model analysis. *Geophysical Research Letters*, *40*, 4194–4198. https://doi.org/10.1002/grl.50813

Frye, K. M., & Marone, C. J. (2002). The effect of particle dimensionality on Granular friction in laboratory shear zones. *Geophysical Research Letters*, *29*(19), 1916. https://doi.org/10.1029/2002GL015709

Gomberg, J. (2010). Slow-slip phenomena in Cascadia from 2007 and beyond: A review. *Geological Society of America Bulletin*, *122*(7-8), 963–978. https://doi.org/10.1130/B30287.1

Gratier, J.-P., & Gueydan, F. (2007). Deformation in the presence of fluids and minerals: Effect of fracturing and fluid-rock interaction on seismic cycles. *Tectonic Faults: Agents of Change on a Dynamic Earth*, *95*, 319–356.

Gu, J.-C., Rice, J. R., Ruina, A. L., & Tse, S. T. (1984). Slip motion and stability of a single degree of freedom elastic system with rate and state dependent friction. *Journal of the Mechanics and Physics of Solids*, *32*(3), 167–196. https://doi.org/10.1016/0022-5096(84)90007-3

Guo, Y., & Morgan, J. K. (2004). Influence of normal stress and grain shape on granular friction: Results of discrete element simulations. *Journal of Geophysical Research*, *109*, B12305. https://doi.org/10.1029/2004JB003044

Guo, Y., & Morgan, J. K. (2006). The frictional and micromechanical effects of grain comminution in fault gouge from distinct element simulations. *Journal of Geophysical Research*, *111*, B12406. https://doi.org/10.1029/2005JB004049

Hanley, K. J., O'Sullivan, C., & Huang, X. (2015). Particle-scale mechanics of sand crushing in compression and shearing using DEM. *Soils and Foundations*, *55*(5), 1100–1112. https://doi.org/10.1016/j.sandf.2015.09.011

Hayman, N. W., Ducloué, L., Foco, K. L., & Daniels, K. E. (2011). Granular controls on periodicity of stick-slip events: kinematics and force-chains in an experimental fault. *Pure and Applied Geophysics*, *168*, 2239–2257. https://doi.org/10.1007/s00024-011-0269-3

Holdsworth, R. E., van Diggelen, E. W. E., Spiers, C. J., de Bresser, J. H. P., Walker, R. J., & Bowen, L. (2011). Fault rocks from the SAFOD core samples: Implications for weakening at shallow depths along the San Andreas Fault, California. *Journal of Structural Geology*, *33*(2), 132–144. https://doi.org/10.1016/j.jsg.2010.11.010

Jiang, M., Zhu, H., & Li, X. (2010). Strain localization analyses of idealized sands in biaxial tests by distinct element method. *Frontiers of Architecture and Civil Engineering in China*, *4*(2), 208–222. https://doi.org/10.1007/s11709-010-0025-2

Karner, S. L., & Marone, C. (2001). Fractional restrengthening in simulated fault gouge: Effect of shear load perturbations. *Journal of Geophysical Research*, *106*(B9), 19,319–19,337. https://doi.org/10.1029/2001JB000263

Landry, J. W., Grest, G. S., Silbert, L. E., & Plimpton, S. J. (2003). Confined granular packings: Structure, stress, and forces. *Physical Review E*, *67*(4), 041303. https://doi.org/10.1103/PhysRevE.67.041303
Leeman, J. R., Saffer, D. M., Scuderi, M. M., & Marone, C. (2016). Laboratory observations of slow earthquakes and the spectrum of tectonic fault slip modes. *Nature Communications*, *7*(11), 104. https://doi.org/10.1038/ncomms11104
Mair, K., & Abe, S. (2008). 3D numerical simulations of fault gouge evolution during shear: Grain size reduction and strain localization. *Earth and Planetary Science Letters*, *274*(1-2), 72–81. https://doi.org/10.1016/j.epsl.2008.07.010
Mair, K., Frye, K. M., & Marone, C. (2002). Influence of grain characteristics on the friction of granular shear zones. *Journal of Geophysical Research*, *107*(B10), 2219. https://doi.org/10.1029/2001JB000516
Mair, K., & Hazzard, J. F. (2007). Nature of stress accommodation in sheared granular material: Insights from 3D numerical modeling. *Earth and Planetary Science Letters*, *259*(3-4), 469–485. https://doi.org/10.1016/j.epsl.2007.05.006
Marketos, G. (2013). Opening up high performance computing to the discrete element method user community (Tech. Rep.). Edinburgh: UK National Supercomputing Service. https://doi.org/10.13140/RG.2.2.33011.43047
Morgan, J. K. (2004). Particle dynamics simulations of rate-and state-dependent frictional sliding of granular fault gouge. *Pure and Applied geophysics*, *161*, 1877–1891. https://doi.org/10.1007/s00024-004-2537-y
Niemeijer, A. R., & Spiers, C. J. (2006). Velocity dependence of strength and healing behaviour in simulated phyllosilicate-bearing fault gouge. *Tectonophysics*, *427*(1-4), 231–253. https://doi.org/10.1016/j.tecto.2006.03.048
Niemeijer, A. R., & Spiers, C. J. (2007). A microphysical model for strong velocity weakening in phyllosilicate-bearing fault gouges. *Journal of Geophysical Research*, *112*, B10405. https://doi.org/10.1029/2007JB005008
Oliphant, T. E. (2006). *Guide to NumPy*. Spanish Fork, UT: Trelgol Publishing.
Plimpton, S. J. (1995). Fast parallel algorithms for short-range molecular dynamics. *Journal of Computational Physics*, *117*(1), 1–19. https://doi.org/10.1006/jcph.1995.1039
Pluymakers, A. M. H., & Spiers, C. J. (2014). Compaction creep of simulated anhydrite fault gouge by pressure solution: Theory vs. experiments and implications for fault sealing. In D. Faulkner, E. Mariani & J. Mecklenburgh (Eds.), *Rock deformation from field, experiments and theory: A volume in honour of Ernie Rutter* (Vol. 409, pp. 107–124). London: Geological Society. https://doi.org/10.1144/SP409.6
Radjai, F., Jean, M., Moreau, J.-J., & Roux, S. (1996). Force distributions in dense two-dimensional granular systems. *Physical Review Letters*, *77*(2), 274–277. https://doi.org/10.1103/PhysRevLett.77.274
Rechenmacher, A. L., Abedi, S., & Chupin, O. (2010). Evolution of force chains in shear bands in sands. *Géotechnique*, *60*(5), 343–351. https://doi.org/10.1680/geot.2010.60.5.343
Richardson, E., & Marone, C. (1999). Effects of normal stress vibrations on frictional healing. *Journal of Geophysical Research: Solid Earth*, *104*(B12), 28,859–28,878. https://doi.org/10.1029/1999JB900320
Rogers, G., & Dragert, H. (2003). Episodic tremor and slip on the Cascadia subduction zone: The chatter of silent slip. *Science*, *300*(5627), 1942–1943. https://doi.org/10.1126/science.1084783
Ruina, A. L. (1983). Slip instability and state variable friction laws. *Journal of Geophysical Research*, *88*(B12), 10,359–10,370. https://doi.org/10.1029/JB088iB12p10359
Scholtès, L., & Donzé, F.-V. (2012). Modelling progressive failure in fractured rock masses using a 3D discrete element method. *International Journal of Rock Mechanics and Mining Sciences*, *52*, 18–30. https://doi.org/10.1016/j.ijrmms.2012.02.009
Scuderi, M. M., Carpenter, B. M., & Marone, C. (2014). Physicochemical processes of frictional healing: Effects of water on stick-slip stress drop and friction of granular fault gouge. *Journal of Geophysical Research: Solid Earth*, *119*, 4090–4105. https://doi.org/10.1002/2013JB010641
Scuderi, M. M., Marone, C., Tinti, E., Di Stefano, G., & Collettini, C. (2016). Precursory changes in seismic velocity for the spectrum of earthquake failure modes. *Nature Geoscience*, *9*(9), 695–700. https://doi.org/10.1038/ngeo2775
Sleep, N. H., & Blanpied, M. L. (1992). Creep, compaction and the weak rheology of major faults. *Nature*, *359*(6397), 687–692. https://doi.org/10.1038/359687a0
Smeraglia, L., Bettucci, A., Billi, A., Carminati, E., Cavallo, A., Di Toro, G., et al. (2017). Microstructural evidence for seismic and aseismic slips along clay-bearing, carbonate faults. *Journal of Geophysical Research: Solid Earth*, *122*, 3895–3915. https://doi.org/10.1002/2017JB014042
Spiers, C. J., Schutjens, P. M. T. M., Brzesowsky, R. H., Peach, C. J., Liezenberg, J. L., & Zwart, H. J. (1990). Experimental determination of constitutive parameters governing creep of rocksalt by pressure solution. *Geological Society, London, Special Publications*, *54*(1), 215–227. https://doi.org/10.1144/GSL.SP.1990.054.01.21
Tenthorey, E., & Cox, S. F. (2006). Cohesive strengthening of fault zones during the interseismic period: An experimental study. *Journal of Geophysical Research*, *111*, B09202. https://doi.org/10.1029/2005JB004122
Tinti, E., Scuderi, M. M., Scognamiglio, L., Di Stefano, G., Marone, C., & Collettini, C. (2016). On the evolution of elastic properties during laboratory stick-slip experiments spanning the transition from slow slip to dynamic rupture. *Journal of Geophysical Research: Solid Earth*, *121*, 8569–8594. https://doi.org/10.1002/2016JB013545
Tordesillas, A., Shi, J., & Muhlhaus, H. B. (2009). Noncoaxiality and force chain evolution. *International Journal of Engineering Science*, *47*(11-12), 1386–1404. https://doi.org/10.1016/j.ijengsci.2008.12.011
Tordesillas, A., Shi, J., & Tshaikiwsky, T. (2011). Stress–dilatancy and force chain evolution. *International Journal of Numerical and Analytical Methods in Geomechanics*, *35*(2), 264–292. https://doi.org/10.1002/nag
Tullis, T. E. (2007). Friction of rock at earthquake slip rates. In *Treatise on Geophysics* (Vol. 4, pp. 131–152). Oxford: Elsevier. https://doi.org/10.1016/B978-044452748-6.00064-X
Van den Ende, M. P. A. (2018). Discrete element method model data of biaxial shear deformation. *GFZ Data Services*. https://doi.org/10.5880/fidgeo.2018.008
Van den Ende, M. P. A., Chen, J., Ampuero, J.-P., & Niemeijer, A. (2018). A comparison between rate-and-state friction and microphysical models, based on numerical simulations of fault slip. *Tectonophysics*, *733*, 273–295. https://doi.org/10.1016/j.tecto.2017.11.040
Van den Ende, M. P. A., Marketos, G., Niemeijer, A. R., & Spiers, C. J. (2018). Investigating compaction by intergranular pressure solution using the discrete element method. *Journal of Geophysical Research: Solid Earth*, *123*, 107–124. https://doi.org/10.1002/2017JB014440